Available online at www.sciencedirect.com
SCIENCE DIRECT®
Acta Materialia 52 (2004) 921–930
Acta MATERIALIA
www.actamat-journals.com

Grain boundary effects on spinodal decomposition II. Discontinuous microstructures

H. Ramanarayan [1], T.A. Abinandanan *

Department of Metallurgy, Indian Institute of Science, Bangalore 560 012, India

Received 18 June 2003; received in revised form 17 October 2003; accepted 21 October 2003

Abstract

We have used a phase field model of a polycrystalline alloy, presented in [Acta Mater. 51 (2003) 4761], to study the effect of enhanced atomic mobility at the grain boundary (GB) on spinodal decomposition (SD) in two dimensional systems. For sufficiently large values of atomic mobility at the GB (M_g), and of GB mobility (L_g), fast decomposition *along* the boundary converts it into a transformation front, whose migration leaves behind a discontinuous microstructure consisting of alternating *A*-rich and *B*-rich lamellae. We present a theory of discontinuous SD under the assumption of a small degree of decomposition in the lamellae (i.e., large values of L_g/M_g). In this limit, for a given M_g, increasing L_g leads to a decrease in the degree of decomposition in the lamellae, but does not alter the lamellar spacing and front velocity, which remain constant. The results from our simulations are in good agreement with these theoretical predictions.

Keywords: Spinodal decomposition; Grain boundaries; Discontinuous transformation; Phase field models

1. Introduction

In [1], hereafter referred to as Paper I, we presented a phase field model for a polycrystalline alloy, and used it to study grain boundary (GB) effects on spinodal decomposition (SD), for systems with constant (position-independent) atomic mobility. The results of Paper I, therefore, are applicable to a restricted class of GB's, such as a twin boundary. In this paper, we study more realistic systems with an enhanced atomic mobility at the GB.

Research in SD in bulk systems has been reviewed in several papers [2–5]. As we remarked in Paper I, a recent trend in SD research is towards elucidating the effect of structural defects on phase separation; these studies, for example, have examined the effects due to a free surface [6–14], dislocations [15], and pre-existing precipitates [16]. In our work, which may be viewed as a part of this trend, we study GB effects on SD.

The new and interesting result from the present study of SD in polycrystalline alloys with GB-enhanced atomic mobility is that, under suitable conditions (identified in Section 3), the GB in the undecomposed alloy becomes a transformation front, whose migration leaves behind a *discontinuous* (or, cellular) microstructure consisting of alternating lamellae of *A*-rich and *B*-rich regions. We have also formulated a theory of this 'mobile front', or discontinuous SD regime, and critically compared its predictions against simulation results.

The paper is organized as follows: We describe briefly, in Section 2, how GB-enhanced mobility is taken into account in our model. We then present, in Section 3, our 2D simulation results. In Section 4, we present a theory of discontinuous SD, and critically compare its results with those from simulations. In Section 5, we show an example of how the GB effects may manifest themselves in a polycrystalline setting. We discuss these results in Section 6, and conclude the paper with a summary in Section 7.

* Corresponding author. Tel.: +91-802-932-676; fax: +91-803-600-472.
E-mail addresses: ram@brown.edu (H. Ramanarayan), abinand@metalrg.iisc.ernet.in (T.A. Abinandanan).
URL: http://metalrg.iisc.ernet.in/~abinand.
[1] Present address: Division of Engineering, Brown University, Providence, RI 02912, USA.

1359-6454/$30.00 © 2003 Acta Materialia Inc. Published by Elsevier Ltd. All rights reserved.
doi:10.1016/j.actamat.2003.10.028

2. Model

The model for a *polycrystalline, two-phase alloy* used in this study is a combination of Cahn–Hilliard [17,18] and Fan–Chen [19] models. We recount it here only briefly (see Paper I for a detailed description), in order to describe how we incorporate a position dependent atomic mobility. Our model uses a composition field $c(\mathbf{r})$, and n orientational order parameter fields η_i $(i = 1, 2, \ldots, n)$ to describe the state of a polycrystalline alloy. Each η_i is associated with a unique grain orientation; from its value of unity inside the ith grain, η_i falls smoothly, over a GB region of finite width, to zero outside this grain. The composition variable c has been scaled so that the compositions of A-rich α and B-rich β phases at equilibrium are $c_\alpha = 0$ and $c_\beta = 1$, respectively.

An instantaneous configuration of the polycrystalline alloy is described by the fields (c, η_i). The free energy F of such an alloy is written as

$$F = N_V \int_V \left[f(c,\eta_i) + \kappa_c (\nabla c)^2 + \kappa_\eta \sum_i (\nabla \eta_i)^2 \right] \mathrm{d}V, \quad (1)$$

where $f(c,\eta_i)$ is the (bulk) free energy per atom in a system with homogeneous fields c and η_i, N_V is the number of atoms per unit volume (assumed to be constant), κ_c and κ_η are the energy coefficients associated with gradients in c and η_i. The evolution of the fields c and η_i are described by, respectively, the Cahn–Hilliard equation [18]:

$$\frac{\partial c}{\partial t} = \nabla \cdot \mathbf{M} \nabla \left[\frac{\delta (F/N_V)}{\delta c} \right], \quad (2)$$

and the Cahn–Allen equation [20]:

$$\frac{\partial \eta_i}{\partial t} = -L \frac{\delta (F/N_V)}{\delta \eta_i}, \quad (3)$$

where **M** is the atomic mobility tensor (which may depend on position) and L is the relaxation coefficient, assumed to be a constant, for η_i.

We use the following form for the bulk free energy density:

$$f(c,\eta_i) = f_c(c) + m(c) \left[0.25 + \sum_i \left(\frac{\eta_i^4}{4} - \frac{\eta_i^2}{2} \right) + \varepsilon \sum_{i,j>i} \eta_i^2 \eta_j^2 \right], \quad (4)$$

with $f_c(c) = A_c c^2 (1-c)^2$, and A_c and ε are constants which set, respectively, the height of the free energy barrier between α and β phases in a single grain, and that between the two grains of the same phase. The factor $m(c)$ couples the fields c and η_i, and is assumed to be of the following form:

$$m(c) = 1 + 0.1c^2 - 6c^2(1-c)^2. \quad (5)$$

This form of $m(c)$ has a minimum at near $c = 0.45$, and $m(1) > m(0)$. As we showed in Paper I, these two features ensure: $\gamma_\beta > \gamma_\alpha$, and $\gamma_i < (\gamma_\alpha + \gamma_c)$ where γ_α, γ_β, γ_c and γ_i are the energies of α-GB, β-GB, coherent and incoherent interfaces, respectively.

Finally, systems with enhanced atomic mobility at GB are studied by using a position-dependent mobility tensor M_{pq}, defined in three-dimensions by

$$M_{pq} = M_b \delta_{pq} + \phi_g \left[M_t \left(t_p^{(1)} t_q^{(1)} + t_p^{(2)} t_q^{(2)} \right) + M_n n_p n_q \right], \quad (6)$$

where the factor $\phi_g = \left[\sum_{i,j>i} \eta_i^2 \eta_j^2 \right]^{\frac{1}{2}}$ is non-zero only at the GB, and is zero inside the grains, $\mathbf{n} = \sum_i \nabla \eta_i / |\sum_i \nabla \eta_i|$ is the unit normal vector to the GB, $\mathbf{t}^{(1)}$ and $\mathbf{t}^{(2)}$ are two mutually perpendicular unit vectors within the boundary plane, M_b is the atomic mobility in the grain interior and, $M_t \geqslant 0$ and $M_n \geqslant 0$ are the GB enhanced atomic mobility in the plane of, and perpendicular to, the GB, respectively. Thus, in a direction parallel to the GB plane, the atomic mobility is $M_b + \phi_g M_t$, and in the normal direction, it is $M_b + \phi_g M_n$; i.e., it takes a value of M_b in the grain interior, and a higher value at the boundary. In this work, we assume $M_n = 0$, and consider enhanced mobility only *along* the GB. Further, in our 2D simulations, we set $\mathbf{t}^{(2)} = \mathbf{0}$.

All the quantities in the above equations are in their non-dimensional form. They are rendered non-dimensional using a characteristic energy $E' = A'_c$, length $L' = \sqrt{\kappa'_c / A'_c}$ and time $T' = L'^2 (c'_\beta - c'_\alpha)^2 / M'_b E'$, where all the primed quantities (such as A'_c) are the dimensional equivalents of their non-dimensional counterparts. This scheme for non-dimensionalization ensures: $A_c = 1$, $\kappa_c = 1$, and $M_b = 1$.

The evolution equations are solved using a semi-implicit spectral method, developed by Zhu et al. [21], who studied the SD in a bulk alloy with a variable **M**. Since the position-dependence of **M** in our model is due to its dependence on η_i, our model is only slightly different from theirs (wherein **M** depends on the local composition); therefore, their method is directly applicable to our model.

In all the simulations whose results are reported here, we have used: $\kappa_\eta = 1$ and $\varepsilon = 2$. For these values, and for our choice of the coupling factor $m(c)$ in Eq. (4), the energies and widths of the four different boundaries (α-GB, β-GB, coherent and incoherent boundaries) are listed in Table 1. In particular, we note: $\gamma_\alpha < \gamma_\beta$, and $\gamma_i < (\gamma_\alpha + \gamma_c)$. As in Paper I, our results in this paper are also presented almost exclusively for a simple system

Table 1
Energies (in units of $N_v \sqrt{A_c \kappa_c}$) and widths (in units of $\sqrt{\kappa_c / A_c}$) of the internal interfaces in the system used in this study

Interface/boundary	Energy	Width
Grain boundary in α	0.732	4.06
Grain boundary in β	0.768	3.87
α–β coherent interface	0.333	4.45
α–β incoherent interface	0.972	4.27

with two grains sharing two planar GB's. The simulations are carried out using a system with 256×512 grid points with periodic boundary conditions, and with $\Delta x = \Delta y = 1$. The time step Δt ranges from 10^{-5} for $M_t = 10^4$, to 0.1 for $M_t = 0$. All the simulations start with a homogeneous alloy of composition $c_0 = 0.5$, on which a uniform fluctuation between $-\delta_c$ and $+\delta_c$ is superimposed; we have used $\delta_c = 0.01$.

3. Results

The model parameter M_t in Eq. (6) is related to M_g, the effective atomic mobility at the GB, and hence, to the GB diffusivity, which is experimentally measurable; similarly, L in Eq. (3) is related to another experimental quantity, the GB mobility L_g, which determines the rate of GB migration under a driving force, such as GB curvature. The linear relationship between M_g and M_t, and that between L_g and L, are derived and used in Section 4.

The values of M_g and L_g span a wide range in real alloys: they have a low value in a highly structured boundary such as a twin boundary, and a large value in high angle grain boundaries. Therefore, we have also studied systems spanning a wide range in terms of M_g and L_g, through simulations in which M_t ranges from 0 to 10^4, and L ranges from 1 to 5×10^4.

We begin by examining the behaviour of the initially planar GB's in two-grain systems. Fig. 1 presents the microstructure in systems with four combinations of M_t and L; for clarity, only a part of the system near one of the original GB's is shown in each figure. It is clear from this figure that there are two distinct behaviours of the original GB. In Fig. 1(a) and (b), the boundary remains stationary (except for a small shift in its position). In Fig. 1(c) and (d), on the other hand, the boundary has migrated over a large distance (compared to the boundary width), leaving behind a *cellular* or *discontinuous* microstructure consisting of alternating *A*-rich and *B*-rich lamellae. In the following subsections, we describe these two behaviours.

3.1. Stationary boundary

In the system in Fig. 1(a), $M_t = 0$ (i.e., there is no enhancement in atomic mobility at the GB), and $L = 1$. The positive difference $(\gamma_\beta - \gamma_\alpha)$ between the GB ener-

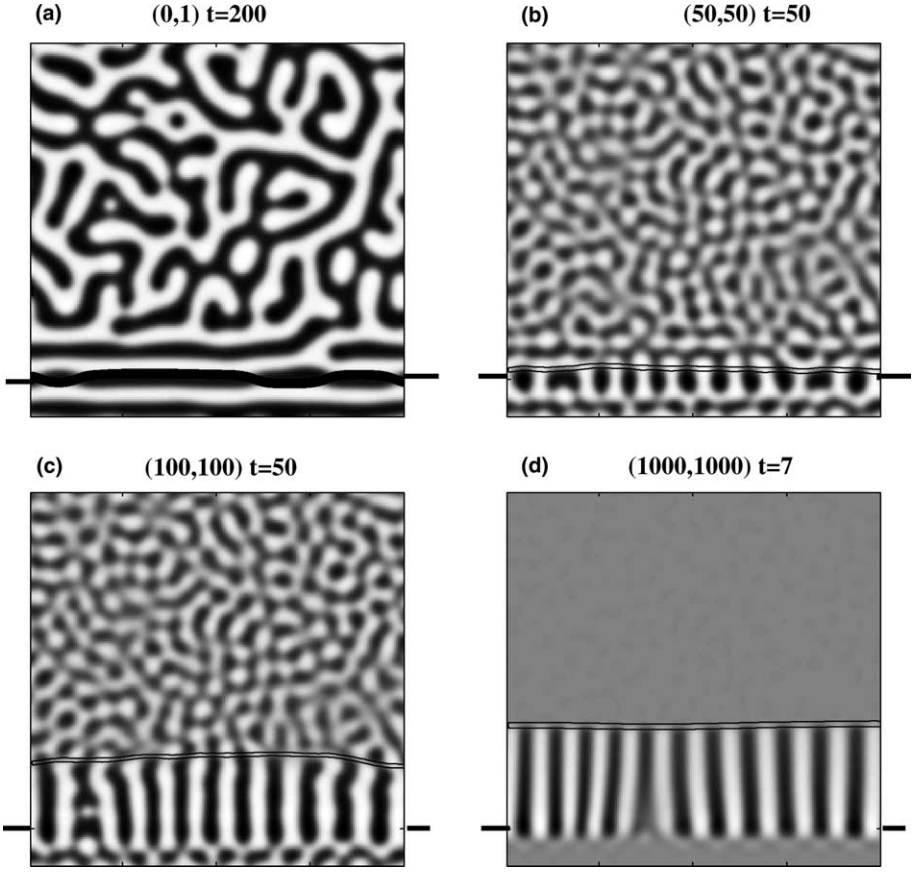

Fig. 1. Microstructural evolution in four different systems with different combinations of (M_t, L) indicated at the top of each figure. For clarity, each figure shows only a part (200×200 grid points) of the system near a planar GB, whose original location is shown by short, horizontal lines on each side. The current location of this boundary is indicated using a double line. In (a) and (b), the GB is stationary, while in (c) and (d), it has migrated considerably. Note that the time in each figure is different.

gies of β and α boundaries leads to the enrichment of species A at the GB. This sets up a composition wave, that travels normal to the GB, leading to the formation of alternating B-rich and A-rich regions (*bands*) on either side of the GB. During this process, the grain interiors undergo normal SD; thus, the final microstructure consists of GB bands coexisting with the normal SD microstructure in the interior.

We have discussed, in Paper I, the factors affecting the formation and number of GB bands in systems with constant mobility. Such a *band formation* is clearly due to the kinetics of enrichment of species A at the GB being faster than that of decomposition along the boundary. The original GB (which would run through the middle of the α band) shifts to one side of the α phase to convert itself into an α–β incoherent boundary; this shift is clearly due to the driving force provided by the formation of an incoherent boundary at the expense of a coherent boundary and an α GB. The boundary does not migrate any further, because such a migration would take it through a band of B-rich region, in which its energy is higher.

Fig. 1(b) shows a variation of a stationary boundary; in this system, a higher value of $M_t = 50$ leads to some decomposition at the GB, while the GB is being enriched with species A. The former leads to alternating A-rich and B-rich *beads* at the GB, while the latter leads to B-rich bands on either side of GB. The final microstructure, therefore, shows A-rich beads at the boundary, surrounded by B-rich bands on either side, coexisting with a normal SD microstructure in the grain interior. Similar to the system in Fig. 1(a), the GB (which would run through the middle of the beads) in this system has also shifted its position to one side of the beads.

3.2. Mobile transformation front and discontinuous SD

Fig. 1(c) and (d) shows the microstructures that result when both M_t and L exceed a critical value. Decomposition along the original GB is much faster than GB-enrichment with species A, and hence does not allow the formation of the B-rich band on either side (as in Fig. 1(b)). So, when the original GB shifts its position to one side of the alternating A-rich and B-rich beads, it encounters an essentially undecomposed parent phase ahead of it. Therefore, it forms a transformation front; i.e., the parent phase decomposes at the front due to the high atomic mobility there. This decomposition causes further migration of the front into the parent phase; the driving force for migration is provided by the lower free energy of the decomposed region behind the front compared to that of the untransformed region ahead of it. The decomposition at the front, coupled with its migration, leads to a discontinuous (or cellular) microstructure consisting of alternating A-rich and B-rich lamellae perpendicular to the front. In the rest of this paper, we refer to this microstructure as 'discontinuous SD microstructure'.

The main difference between Fig. 1(c) and (d) is in the kinetics of migration of the transformation front. In Fig. 1(c), it is slow enough to allow the grain interiors to undergo normal SD; thus, the system exhibits a mixture of normal SD and discontinuous SD microstructures. In contrast, in Fig. 1(d), the front migration is so fast (because of the very large values of M_t and L used in this simulation) that it traverses the entire grain before normal SD can take place in the grain interior.

In a log–log plot of M_t and L in Fig. 2, we have identified the conditions for stationary and mobile boundaries. Since decomposition along the boundary is a pre-requisite for the front formation and its subsequent migration, clearly M_t has to exceed a critical value, which is estimated from this figure to be about $M_{t,c} \approx 100$ for the system under study. Further, the GB mobility also should exceed a critical value: for example, for $M_t = 100$, a stationary boundary (with beads) results if $L = 10$, while a mobile front is formed if $L = 100$. The critical values of M_t and L can be lowered if the boundary is curved; we have confirmed [22] that a system with an initially curved GB forms a transformation front even for $M_t = 50$ and $L = 50$; curvature provides a driving force for the boundary to migrate, thereby hindering GB-enrichment with species A, and leading to an easier formation of the front.

In Fig. 3, we plot the average position of the transformation front with time for systems which exhibit only a discontinuous microstructure. In these systems, the front migration is so fast, due to large values of $M_t \geqslant 10^3$ and $L \geqslant 10^3$, that it is not hindered by normal

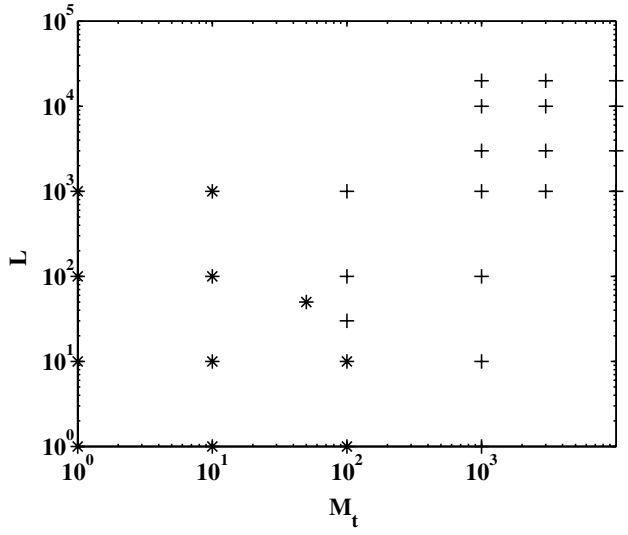

Fig. 2. Dependence of the behaviour of the original GB on M_t and L: stationary boundary (marked *) and migrating transformation front (marked +). A critical value of $M_t \approx 100$ appears to be necessary for the formation of a transformation front.

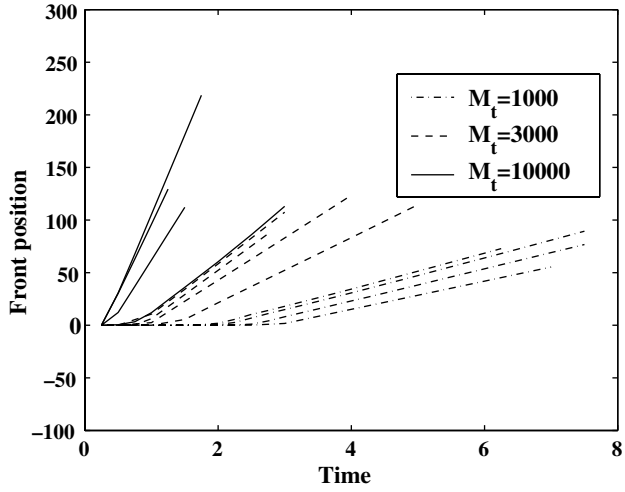

Fig. 3. Front position as a function of time: each set of four curves corresponds to a particular value of M_t: 10^3 (dot-dashed), 3×10^3 (dashed), and 10^4 (solid). In each set, the curves with increasing slope at later times correspond to increasing values of L: 10^3, 3×10^3, 10^4 and 2×10^4. Note the initial transient in each case, followed by a straight line, whose slope yields the front velocity.

SD in the grain interiors. For each system in this figure, the straight line behaviour for late times shows that front migration (growth) occurs at a constant velocity; the initial transient is due to early stage decomposition along the boundary and formation of the transformation front.

In Fig. 4, we plot the composition profile parallel to the front at a distance behind the front, for two different systems: the one with $M_t = 10^4$, $L = 10^3$ (top) exhibits a larger interlamellar spacing than that with $M_t = 10^3$, $L = 2 \times 10^4$. Also, the degree of decomposition is higher, and the front migration is slower (see Fig. 3), in the former than in the latter.

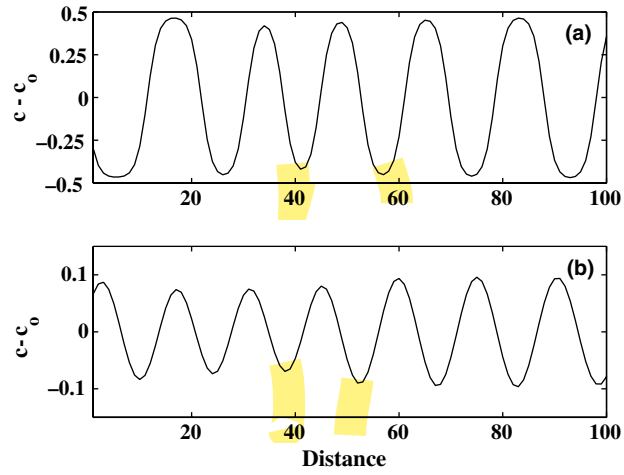

Fig. 4. Profile of $(c - c_0)$ behind (and in a direction parallel to) the migrating front for (M_t, L) being (a) $(10^4, 10^3)$ and (b) $(10^3, 2\times10^4)$. There are more lamellae in (b) than in (a); further, lamellae in (b) display a smaller degree of decomposition than those in (a). Note the different scales for the y-axis in (a) and (b).

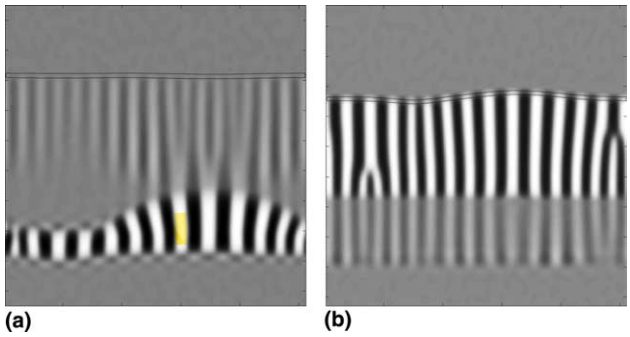

Fig. 5. Response of the migrating front to a sudden change in simulation conditions: left figure is for a change in (M_t, L) from $(10^3, 10^4)$ to $(10^4, 10^3)$, and the right figure is for the reverse change.

It is clear from Figs. 3 and 4 that front migration in each system (with a particular set of values for M_t and L) is characterized by a unique combination of the three quantities: lamellar spacing λ, front velocity v, and degree of decomposition in the lamellae. In order to test this uniqueness, we performed a two-step simulation: starting with $(M_t, L) = (10^4, 10^3)$, we allowed steady-state front migration for a certain time, at which we imposed a sudden change in conditions to $(M_t, L) = (10^3, 10^4)$. The result of this simulation is shown in the left figure of Fig. 5, which shows that the system does indeed adjust itself (by producing finer lamellae with a smaller degree of decomposition) to the new conditions. The right figure in Fig. 5 illustrates the reverse change in front characteristics following a change in conditions in the reverse direction from $(M_t, L) = (10^3, 10^4)$ to $(10^4, 10^3)$.

4. Theory of discontinuous SD

A general theory of discontinuous SD would require a detailed account of the diffusion process within the moving front, and hence, is difficult to formulate. However, Fig. 4 provides an insight: the composition profile $(c - c_0)$ exhibits a small amplitude in Fig. 4(b), and hence may be approximated as a sinusoidal wave. Our theory is developed using this insight, together with Cahn's original ideas on front migration during discontinuous precipitation [23].

4.1. Preliminaries

The quantities that enter the theory are the GB mobility (L_g), and the *effective* atomic mobility along the GB (M_g); as we noted at the beginning of Section 3, these quantities depend linearly on our model parameters L and M_t, respectively. For the linear relationship $L_g = K_L L$, we obtain K_L as follows: In a system with, say, two α grains with two planar GB's, if the atoms in the first grain have a (slightly) lower free energy than those

in the second, then the first grain would grow at the expense of the second; i.e., the GB's would migrate. By measuring the GB velocity, $v_{gb} = -L_g \Delta G$, in a simulation (using predetermined ΔG and a certain value of L), L_g can be determined, and hence, so can K_L. Using this procedure, we estimate $K_L = L_g/L$ for our system to be 2.5, so that we have:

$$L_g \approx 2.5L. \tag{7}$$

For determining K_M in the relationship $M_g = K_M M_t$, we take M_g, the (effective) atomic mobility at the GB, to be given by the weighted average of M_p, the atomic mobility *along* the boundary, over the GB width:

$$M_g = \frac{1}{w}\int_{-\infty}^{\infty} M_p \, ds,$$

where s is the distance variable in the direction normal to the GB plane, and $M_p = M_b + \phi_g M_t$ in our model. Since our theory is applicable for systems in which $\phi_g M_t \gg M_b$, we have $M_p \approx \phi_g M_t$. Using this approximation, and evaluating the integral on the RHS numerically, we get:

$$M_g w \approx 0.73 M_t. \tag{8}$$

4.2. Driving force for front migration

Following Cahn [23], we postulate that v, the front velocity, is proportional to (with L_g being the proportionality constant) a driving force $\Delta G = G_d - G_0$. The free energy difference ΔG is between $G_d = (1/\lambda)\int_0^\lambda [f_c(c) + \kappa_c(\partial c/\partial x)^2]dx$, the free energy per atom of the decomposed (lamellar) region behind the front, and $G_0 = (1/\lambda)\int_0^\lambda f_c(c_0)dx = f_c(c_0)$, that of the untransformed region ahead of it; x is the distance variable along a direction parallel to the front (assumed to be planar), and λ is the lamellar spacing or wavelength. Thus, we have the following equation for the front velocity:

$$v = -L_g \Delta G. \tag{9}$$

Motivated by Fig. 4, we write the composition profile $(c - c_0)$ in the decomposed region behind the front as a cosine wave with an amplitude c_k;

$$c - c_0 = c_k \cos(kx), \tag{10}$$

where $k = 2\pi/\lambda$ is the wave number. Clearly, the degree of decomposition $\langle (c-c_0)^2 \rangle$ is linearly related to c_k^2:

$$\langle (c-c_0)^2 \rangle = \frac{1}{\lambda}\int_0^\lambda (c-c_0)^2 dx = \frac{c_k^2}{2}. \tag{11}$$

For small values of $(c - c_0)$, we can use the approximation $f_c(c - c_0) = f_c(c_0) + (c - c_0) f_c'(c_0) + (1/2)(c - c_0)^2 f_c''(c_0)$, and evaluate ΔG exactly:

$$\Delta G = (1/\lambda)\int_0^\lambda \left[\frac{(c-c_0)^2}{2} f_c''(c_0) + \kappa_c c_k^2 k^2 \sin^2(kx)\right] dx = \frac{c_k^2 g(k)}{4},$$

where the function $g(k)$ is given by $g(k) = f_c''(c_0) + 2\kappa_c k^2$. Substituting for ΔG in Eq. (9), we get the following expression for v:

$$v = \frac{-L_g c_k^2 g(k)}{4}. \tag{12}$$

4.3. Diffusion within the front

We use an approximate treatment of diffusion within the moving boundary (front). For a front of width w, $\Delta t = w/v$ is the time available for each species to redistribute itself into the A-rich and B-rich lamellae (see Fig. 6). Confining our attention to the boundary segment spanning half a wavelength $0 \leqslant x \leqslant \lambda/2$, the flux of B atoms along the boundary, J, evaluated at $x = \lambda/4$ (where $c = c_0$) is given by

$$J(\lambda/4) = -M_g [\nabla_t \mu]_{\lambda/4}, \tag{13}$$

where $[\nabla_t \mu]_{\lambda/4}$ is the chemical potential gradient along the boundary, evaluated at $x = \lambda/4$. The amount of B atoms thus transported in time Δt is

$$J\Delta t = \frac{-M_g w [\nabla_t \mu]_{\lambda/4}}{v}. \tag{14}$$

This amount, $J\Delta t$, of B atoms is used in building up an excess concentration over c_0 in the region $0 \leqslant x \leqslant \lambda/4$. Therefore, we also have the following relation:

$$J\Delta t = c_k \int_0^{\lambda/4} \cos(kx) dx = \frac{c_k}{k}. \tag{15}$$

Equating the RHS of the previous two equations, we get:

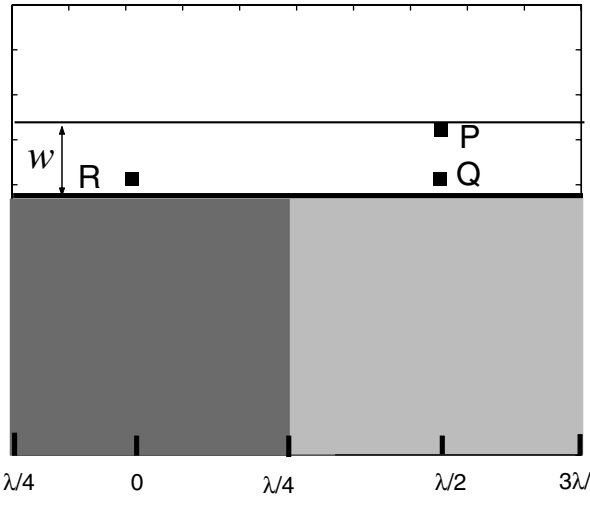

Fig. 6. A schematic figure showing a B-rich lamella (dark gray region) and an A-rich lamella (light gray region) with the transformation front, of width w, at their tip. Further growth of the lamellae is achieved by the upward migration of the transformation front. The middle of the B-rich lamella is used as the origin ($x = 0$) in the theory.

$$\frac{-M_g w[\nabla_t \mu]_{\lambda/4}}{v} = \frac{c_k}{k}. \quad (16)$$

For the chemical potential gradient, we use the approximation $[\nabla_t \mu]_{\lambda/4} = 2\Delta\mu/\lambda$, where $\Delta\mu = \mu(x=0) - \mu(x=\lambda/2)$. In Fig. 6, at $x = 0$, the location at **R** is where μ is lower, and hence B atoms migrate towards **R**; thus, we assume $\mu(x=0) \approx \mu(\mathbf{R})$.

For $\mu(x=\lambda/2)$, however, there is a continuum of choices across the width of the front; for example, one could evaluate $\mu(\lambda/2)$ at the locations **P** or **Q** (which lead to fairly simple results, as shown below); each would lead to a different value for $\Delta\mu$. Consider the point **P**, which the moving front (of finite thickness) has just entered; clearly, the region at and near **P** is in an undecomposed state of composition $c = c_0$. For this choice of $\mu(\lambda/2) \approx \mu(\mathbf{P})$, we get:

$$[\Delta\mu]_{\mathbf{P}}^{\mathbf{R}} = \left[f_c'(c) - 2\kappa_c \frac{\partial^2 c}{\partial x^2}\right]_{\mathbf{R}} - \left[f_c'(c)\right]_{\mathbf{P}} = c_k g(k),$$

where we have used the approximation: $f_c'(c_0 + c_k) = f_c'(c_0) + c_k f_c''(c_0)$.

On the other hand, consider the location **Q**, which the front is about to exit; clearly, the region at and near **Q** is in a decomposed state with a composition $c = c_0 - c_k$. Thus, for this choice of $\mu(\lambda/2) \approx \mu(\mathbf{Q})$, and using a procedure similar to that for location **P**, we get:

$$[\Delta\mu]_{\mathbf{Q}}^{\mathbf{R}} = 2c_k g(k).$$

The above two possibilities for $\Delta\mu$ may be written in the following general form:

$$\Delta\mu = q_\mu c_k g(k), \quad (17)$$

where the factor $q_\mu = 1$ or $q_\mu = 2$ corresponds to evaluating $\mu(\lambda/2)$ using, respectively, the point **P** or **Q**.

Substituting for $[\nabla_t \mu]_{\lambda/4} = 2\Delta\mu/\lambda$ from Eq. (17) into Eq. (16), we obtain

$$v = \frac{-M_g k^2 q_\mu w g(k)}{\pi}. \quad (18)$$

Interestingly, this equation does not contain c_k anywhere; it drops out because, while it appears on the RHS of Eq. (16) to account for the extent of decomposition, it also appears in the LHS for $\Delta\mu$, the driving force, in Eq. (17).

We now have two equations, Eqs. (12) and (18), involving v, c_k and k which characterize the migrating front; in the 3D space spanned by the three variables, these equations define two intersecting surfaces. Any point that lies on the line of intersection could, in principle, describe an *operating state* (i.e., a combination of v, k and c_k) of the migrating front. We therefore need another condition to describe the *unique* operating state observed in each simulation. In theories of eutectoid transformation and cellular precipitation (see, for example, [23]), a 'maximum growth rate' condition is often used; we too use this condition.

Since Eq. (18) does not contain c_k, the projection of the line of intersection (of the surfaces given by Eqs. (12) and (18)) on the v–k plane is the same as the curve $v(k)$ described by Eq. (18). This projection is shown in Fig. 7. Thus, using the maximum growth rate condition on this curve, we get k^*, which is used in Eq. (18) to get v^*; use of these two quantities in Eq. (12), and Eq. (11) yields the corresponding extent of decomposition, $\langle (c - c_0)^2 \rangle^*$.

4.4. Predictions for discontinuous SD

Our theory is applicable for a regime in which significant front migration occurs under small driving forces (large L_g) arising from a small amplitude decomposition (small M_g). Since L_g and M_g used in theory are linearly related to, respectively, L and M_t used in the simulations (see Eqs. (7) and (8)), our theory is applicable for the regime of large values of L/M_t. For this regime, the theoretical predictions are the following:

1. The wavelength of decomposition (lamellar spacing), $\lambda^* = 4\pi\sqrt{-\kappa_c/f''(c_0)}$, is constant, independent of L or M. Interestingly, λ^* is the same as the wavelength of the fastest growing fluctuations during early stages of SD in bulk alloys [18].
2. The scaled velocity $[v^*/M_t]$ is constant. The value of this constant for our system (see Eqs. (8) and (18)) is $-[0.73 q_\mu k^{*2} g(k^*)/\pi]$.
3. The degree of decomposition, $\langle (c - c_0)^2 \rangle^*$, is inversely proportional to L/M_t.

Thus, for a given M_t, increasing L does not affect the lamellar spacing or front velocity; however, the lamellae would exhibit a smaller degree of decomposition.

4.5. Comparison between theory and simulations

All the results from our simulations of front migration for different combinations of M_t and L are shown in

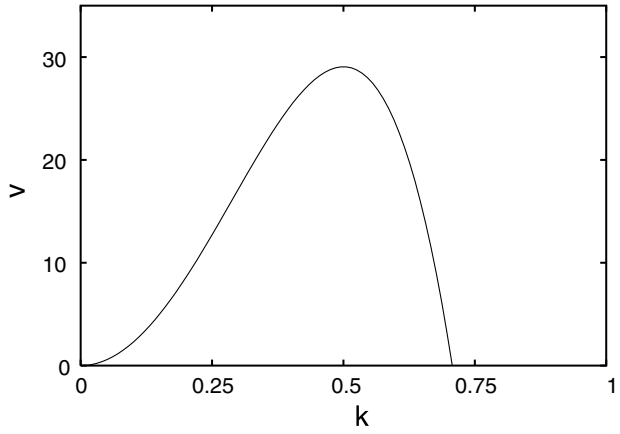

Fig. 7. The projection of the line of intersection of the two surfaces $v_1(k, c_k)$, given by Eq. (12) and $v_2(k, c_k)$, given by Eq. (18), on the v–k plane, for a system with $c_0 = 0.5$, $M_t = 10^3$, and $q_\mu = 1$. Since Eq. (18) is independent of c_k, this projection is simply a plot of the same equation.

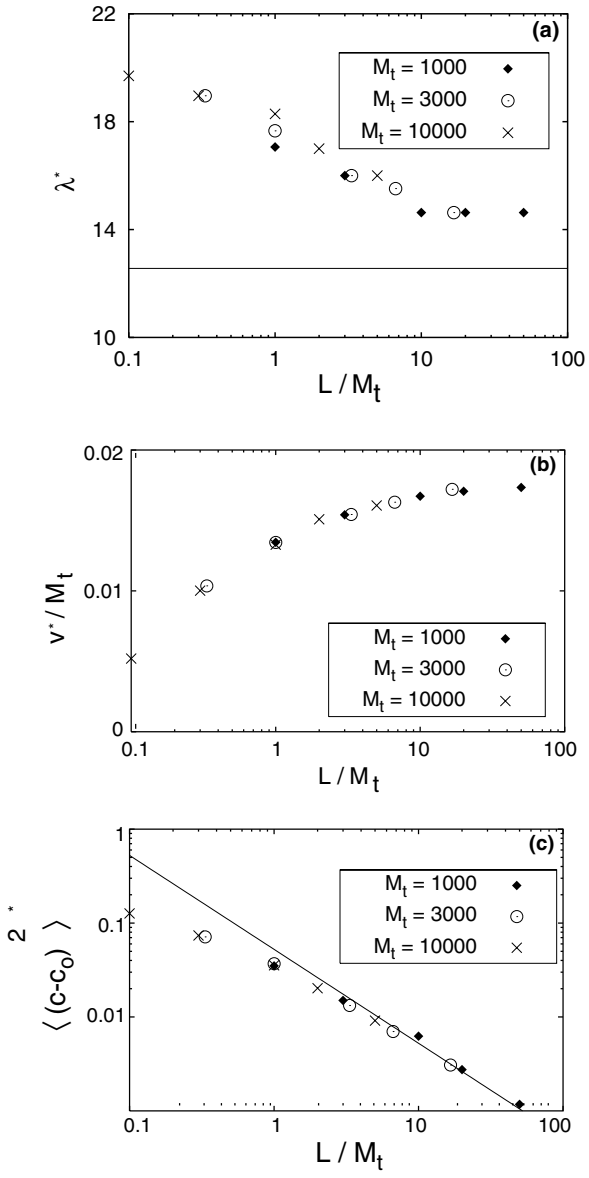

Fig. 8. Plots of (a) Interlamellar spacing λ^*, (b) v^*/M_t, and (c) $\langle (c-c_0)^2 \rangle^*$ against $L/(M_t)$. The horizontal line in (a) represents the theoretical prediction. The straight line in (c), with a slope of −1, is a guide to the eye.

Fig. 8, in which the three front characteristics (the wavelength λ^*, the scaled velocity $[v^*/M_t]$, and degree of decomposition $\langle (c-c_0)^2 \rangle^*$) are plotted against L/M_t. As already mentioned, our theory is applicable for large values of L/M_t. It is clear from this figure that, in this regime, both λ^*, and $[v^*/M_t]$ do indeed tend towards constant values. More importantly, in a log–log plot of $\langle (c-c_0)^2 \rangle^*$ against L/M_t, the simulation data for the large (L/M_t) regime do exhibit a slope of −1. Thus, the trends in the simulation data are in good agreement with those predicted by the theory. However, there are quantitative differences: the theory underestimates λ^* by 20%, and overestimates the velocity by a factor of between 60% and 220% (corresponding to, respectively, $q_\mu = 1$ and $q_\mu = 2$). The quantitative differences between theory and simulations stem essentially from the approximate way in which the theory accounts for diffusion in the migrating front. Further, we have implicitly assumed that the migrating front has the same properties (order parameter profiles and width) as an equilibrium incoherent boundary; in reality, however, the front is a boundary between the untransformed and the partially transformed regions, neither of which is in equilibrium with each other.

Before concluding this section, we turn briefly to the front characteristics for small (L/M_t), outside the regime of validity of the theory. It is clear from Fig. 8 that, for systems with a constant value of M_t, a decreasing L leads to coarser, slower-growing and more decomposed lamellae. Clearly, a slower front migration implies more time for diffusion; thus, a greater degree of decomposition is achieved over wider lamellar spacings. The results for this regime are along expected lines, and are similar to those for discontinuous precipitation and eutectoid transformation [23].

5. Spinodal decomposition in a polycrystal

Fig. 9 shows the microstructural evolution in a polycrystal with $M_t = 1000$ and $L = 1000$; it is clear that almost all the boundaries form a transformation front readily, indicating that all the results presented so far are applicable to this polycrystal. The presence of triple points and of boundaries with different curvatures leads to additional features, which are summarized below:

- Different fronts behave differently. For example, the boundaries (marked 1) around an initially small grain migrate inwards very fast, leading to a small degree of decomposition. On the other hand, the GB (marked 2), with a smaller initial curvature, migrates slower and allows a greater degree of decomposition.
- Decomposition at different parts of the same GB (marked 3) may lead to transformation fronts propagating in opposite directions.
- The front migration is influenced by the presence of other boundaries, their movement, and by the constraints imposed by the triple points. A part of the boundary (marked 3) which appears to be migrating in the south-westerly direction at $t = 4$, has clearly reversed its direction of migration by $t = 8$.
- The above constraints also lead to a different behaviour of the same front at different times; see, for example, the boundaries marked 4, with their ever changing lamellar spacing. This implies that transformation fronts in polycrystals may not exhibit steady state behaviour.

These features are novel and interesting; however, their applicability to a real polycrystal is limited due to

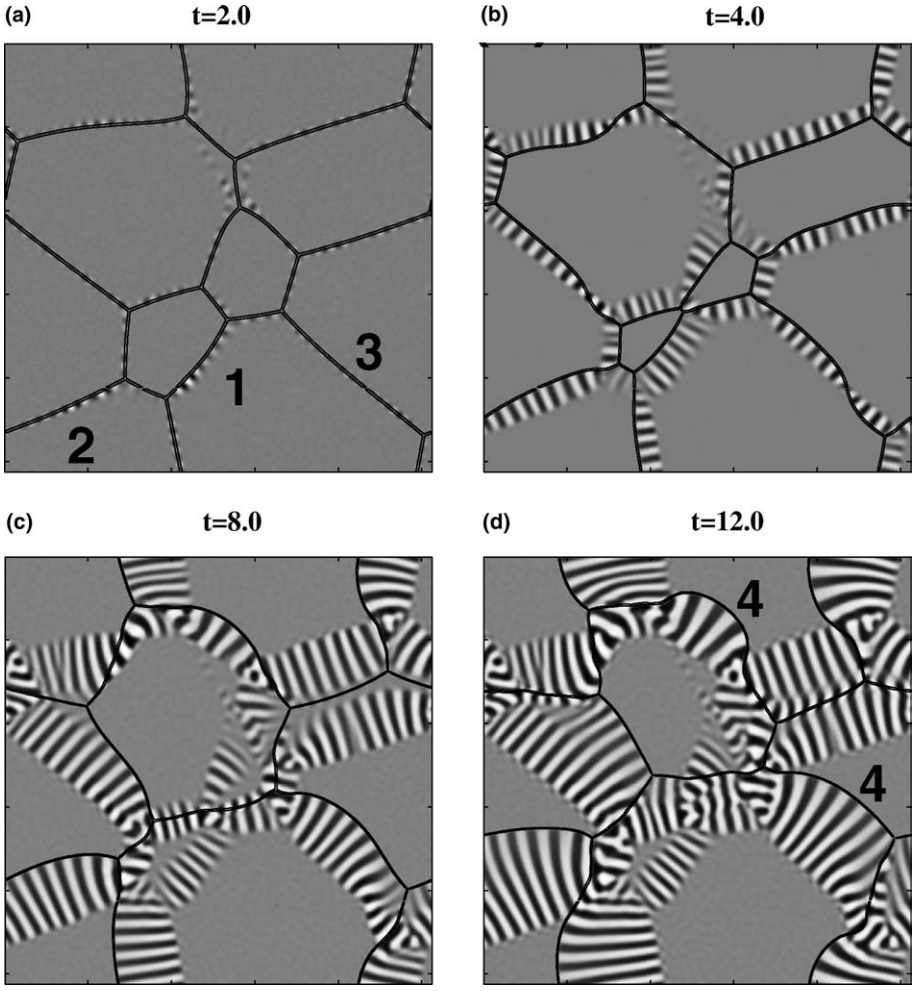

Fig. 9. Microstructural evolution in a polycrystalline alloy of composition $c_0 = 0.5$ in system IIb with $M_t = L = 10^3$. Time is indicated on top of each microstructure. This simulation used a 512×512 grid.

the following considerations: First, they have been observed in a system with a small grain size, of the order of few tens of the characteristic interlamellar spacing. In systems with a large grain size, these features are likely to be rarer. Further, we have studied only one polycrystalline system, with a particular combination of boundary energies in Table 1; only a systematic study of the effect of a change in this combination would allow us to determine how common these features are in real systems. We have not attempted such a study, which would require many simulations with a large number of grains, because of computational limitations.

6. Discussion

6.1. Discontinuous SD and discontinuous precipitation

The important contributions of the present study are: (a) identification of a discontinuous SD mechanism that produces a lamellar microstructure in systems with large values of M_t and L, and (b) a theory of discontinuous SD for systems with large values of L/M_t; the simulation results are in good agreement with those from our theory.

Note that we have used the term 'discontinuous SD' rather than 'discontinuous precipitation' (DP) to describe the phenomenon that produces a lamellar microstructure in our simulations. We justify our terminology by explaining the difference between DP and discontinuous SD as follows; this difference is essentially the same as that between SD and precipitation in bulk systems. In DP, one of the lamellae must be of the precipitate phase, whose composition is significantly different from that of the matrix. In other words, the two phases have a 'well-formed' interface, whose energy may be assumed to be constant, as in the theories of DP [23–26]. In discontinuous SD, on the other hand, the lamellae (particularly in systems with large L_g/M_g) are due to a composition wave of small amplitude; in Gibb's terminology [27], such a variation in c is 'small in degree, but ... great in extent'. Further, our simulations show that the amplitude c_k may be arbitrarily small, for an arbitrarily large L. Therefore, the coherent interfaces between A-rich and B-rich lamellae in our simulations

are, in Cahn's words [18], 'incipient *surfaces* [interfaces]', and may have an arbitrarily small interfacial energy.

This additional freedom of the system to produce lamellae with incipient interfaces, and hence with a low (and variable) interfacial energy leads to an interesting difference in the predictions of theories of DP and discontinuous SD. Cahn's theory of DP [23] predicts, in the limit of large GB mobility (L), an increase in lamellar spacing with increasing L. In our theory of discontinuous SD, on the other hand, the interlamellar spacing λ^* is constant for large L/M_t; an increase in L in this regime leads to a front with lamellae of the same spacing but a smaller interfacial energy due to a smaller degree of decomposition.

6.2. Experimental evidence for discontinuous SD

There are reports of discontinuous (cellular, lamellar) microstructures in spinodally decomposing systems; interestingly, the origin of these microstructures are often attributed to DP; based on the above discussion, they are more likely due to discontinuous SD.

Several experimental studies have reported the coexistence of discontinuous microstructures and normal spinodal microstructure within the grains. Examples include Cu–Ni–Fe [28] and Cu–Ni–Sn [29] alloys. Thus, these systems belong to the same class as that shown in Fig. 1(c). On the other hand, for a system that exhibits only a discontinuous microstructure (as in Fig. 1(d)), we could find only one example: Au–Ni system [30], in which aging above the coherent spinodal does not allow any decomposition in the grain interior. We emphasize that, these studies present only a visual evidence (or a brief description) of discontinuous microstructures; this is because their main focus is on normal SD in the grain interior. We have not been able to find a quantitative study of these microstructures, in terms of the front velocity, interlamellar spacing and degree of decomposition.

7. Conclusions

(1) We have studied, using computer simulations based on a phase field model of polycrystalline alloys, the effect of GB-enhanced atomic mobility (M_g), and GB mobility (L_g) on SD.
(2) For low values of M_g (and also of L_g), the GB remains stationary, and exhibits either bands or beads that are richer in A, the component with the lower GB energy. On either side of the original GB, a B-rich band is formed.
(3) For large values of M_g and L_g, the GB forms a transformation front, whose migration leaves behind it a discontinuous SD microstructure consisting of alternating A-rich and B-rich lamellae.
(4) We have presented a theory of discontinuous SD, applicable for large values of L_g/M_g. Its results on the front velocity, degree of decomposition and interlamellar spacing are in good agreement with those from our simulations.

Acknowledgements

We thank the Council of Scientific and Industrial Research, Government of India, for financial support for this work. We gratefully acknowledge fruitful discussions with Professors V. Jayaram, P.W. Voorhees, P. Bellon and F. Haider.

References

[1] Ramanarayan H, Abinandanan TA. Acta Mater 2003;51:4761.
[2] Binder K. Phase transformations in materials. In: Kostorz G, editor. Transformation in materials. Weinheim: Wiley-VCH; 2001.
[3] Binder K. Materials science and technology. In: Haasen P, editor. Transformation in materials, vol. 5. Weinheim: VCH; 1991.
[4] Fratzl P, Penrose O, Lebowitz JL. J Stat Phys 1999;95:1429.
[5] Bray AJ. Adv Phys 1994;43:357.
[6] Marko JF. Phys Rev E 1993;48:2681.
[7] Bastea S, Puri S, Lebowitz JL. Phys Rev E 2001;63:041513.
[8] Frisch HL, Nielaba P, Binder K. Phys Rev E 1995;52:848.
[9] Puri S, Binder K. Phys Rev Lett 2001;86:1797.
[10] Puri S, Binder K, Frisch HL. Phys Rev E 1997;56:6991.
[11] Puri S, Binder K. J Stat Phys 1994;77:145.
[12] Fischer HP, Maass P, Dieterich W. Phys Rev Lett 1997;79:893.
[13] Geng C, Chen L-Q. Surf Sci 1996;355:229.
[14] Geoghegan M, Ermer H, Jungst G, Krausch G, Brenn R. Phy Rev E 2000;62:940.
[15] Hu SY, Chen L-Q. Acta Mater 2001;49:463.
[16] Moore KT, Johnson WC, Howe JM, Aaronson HI, Veblen DR. Acta Mater 2002;50:943.
[17] Cahn JW, Hilliard HE. J Chem Phys 1958;28:258.
[18] Cahn JW. Acta Metall 1961;9:795.
[19] Fan D, Chen L-Q. Acta Mater 1997;45:3297.
[20] Allen SM, Cahn JW. Acta Metall 1979;27:1085.
[21] Zhu J, Chen L-Q, Shen J, Tikare V. Phys Rev E 1999; 60:3564.
[22] Ramanarayan H. PhD Thesis, Indian Institute of Science, 2003.
[23] Cahn JW. Acta Metall 1959;7:18.
[24] Turnbull D. Acta Metall 1955;3:55.
[25] Hillert M. Metall Trans 1972;3:2729.
[26] Hillert M. Acta Metall 1982;30:1689.
[27] Gibbs JW. In: Collected Works, vol. 1. New Haven: Yale University Press; 1948. p. 256.
[28] Gronsky R, Thomas G. Acta Metall 1975;23:1163.
[29] Zhao J, Notis M. Met Trans A 1999;30A:707.
[30] Gust W, Predel B, Nguyen-Tat T. Z Metall 1976;67:110.